Journal of Hydrology: Regional Studies 50 (2023) 101550

Contents lists available at ScienceDirect

Journal of Hydrology: Regional Studies

journal homepage: www.elsevier.com/locate/ejrh

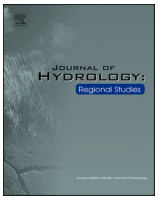

Quantifying groundwater recharge in the Venetian high plain between the Brenta and Piave Rivers through integrated surface–subsurface hydrological modeling

Beatrice Gatto, Davide Furlanetto, Matteo Camporese *, Tommaso Trentin, Paolo Salandin

Department of Civil, Environmental, and Architectural Engineering, University of Padova, Italy

ARTICLE INFO

Keywords:
Unconfined aquifer
CATHY
Irrigation
Finite element method

ABSTRACT

Study region: Venetian high plain between the Brenta and Piave Rivers, Northeast Italy.
Study focus: Groundwater recharge is the process by which aquifers, i.e., the groundwater reservoirs, are replenished. In many regions, recharge fluxes are currently declining due to more frequent hydroclimatic extreme events and unsustainable land use management. In this study, CATHY (CATchment Hydrology), an integrated surface–subsurface hydrological model (ISSHM), is used to estimate current and future recharge fluxes in a study area that represents an important source of drinking water supply for the Treviso province (Veneto Region, Northeast Italy). In particular, we aim to evaluate the impacts on recharge of a scenario with changed irrigation management, planned in compliance with European directive indications, to decrease water withdrawals from the Piave River and preserve its ecological flow. The model was first calibrated through a combination of FePEST and the Shuffled Complex Evolution algorithm, whereby both the bottom of the unconfined aquifer and the hydraulic conductivity field were tuned. After a validation step, the resulting model was used to simulate a scenario in which the flood irrigation method, currently the most widespread in the study area, is fully replaced by sprinkler irrigation.
New hydrological insights for the region: Our results show that, in response to a 50 % decrease in water withdrawn from the Piave River, the total recharge decreases by about 10 %, with a local reduction in groundwater head, mainly limited in wells located in the area directly affected by the conversion of the irrigation technique. The model suggests that most of the recharge fluxes occur in irrigated areas where the hydraulic conductivity is higher. Overall, this work resulted in the development of an ISSHM capable to reproduce groundwater dynamics and its drivers at high resolution and large scale. Although it can still be improved, the model represents a useful tool to investigate possible responses of the considered hydrosystem to future land use and climate change.

1. Introduction

Groundwater accounts for almost 99 % of the available liquid freshwater present on Earth and is the main source of drinking water

* Corresponding author.
E-mail address: matteo.camporese@unipd.it (M. Camporese).

https://doi.org/10.1016/j.ejrh.2023.101550
Received 28 July 2023; Received in revised form 30 September 2023; Accepted 11 October 2023

and irrigation (Xiong et al., 2022). In pristine conditions, the high quality of groundwater is guaranteed by natural soil processes such as attenuation, retention, and adsorption of non-anthropogenic contaminants. Starting with the Industrial Revolution, disturbances in groundwater flow and quality began to occur at large scales (Edmunds and Shand, 2008). Since then, new pollutants, unsustainable land use, aquifer overexploitation, and climate changes have led to the so-called *global groundwater crisis* (Famiglietti, 2014). While in industrialized countries clean and safe drinking water is often taken for granted, in the rest of the world it is unevenly distributed (Gleick and Cooley, 2021). According to a new *United Nations World Water Development Report* around 2 billion people worldwide still do not have access to clean and safe water and at least 3.6 billion people experience water scarcity for at least one month of the year (Boretti and Rosa, 2019; UNESCO, 2023) with some estimates reaching up to 4.3 billion (Mesfin and Arjen, 2016). Sanitation conditions are often inadequate and cause in a year 3.4 million deaths (Osiemo et al., 2019).

Climate change and unsustainable rates of water consumption are worsening these issues. For instance, climate change affects drinkable water due to higher temperatures leading to increased growth of new parasites and survival of bacteria (Jeon et al., 2019), while altered weather patterns and water cycles around the world are causing more frequent extreme events such as droughts and floods (Richts et al., 2016; Mahlalela et al., 2019), with associated reductions in groundwater recharge.

Sustainable management of aquifers relies on a delicate balance between input fluxes, i.e., snow, rainfall, losing rivers, and sometimes excess irrigation, and outputs fluxes, including withdrawals for economic, social, and environmental development. This equilibrium, which in some cases took centuries to be achieved, can be easily disrupted by unsustainable human activities and extreme climate events that lead to year-by-year recharge variability (Gumuła-Kawęcka et al., 2022). If the amount of water extracted exceeds the amount of water replenishing the aquifer, the result is a groundwater depletion that can imply less drinking water supply, reduction in groundwater quality, salinization, subsidence, and strong impacts on the environmental ecosystems (Konikow and Kendy, 2005). For this reason, there is a compelling need to carefully evaluate all the terms of the aquifer water balance, to ensure their sustainable management.

The Venetian high plain between the Piave and Brenta Rivers, the region in northeast Italy where the study area of this research is located, is characterized by an agricultural tradition that has endured for centuries. The irrigation method that has generally been used there is flood irrigation. According to recent European Union directives and Italian legislation (*European Drinking Water Directive 2020/2184*; Deflussi Ecologici Decree 30/, 2017), this kind of irrigation is no more sustainable, and is gradually being converted into sprinkler irrigation, which is supposed to be more efficient and should result in less water withdrawals from rivers, ensuring their ecological flow. However, excess irrigation in the Venetian high plain represents an important fraction of groundwater recharge (Dal Prà A. et al., 1996; Fabbri et al., 2016). Therefore, quantifying the impacts of changing irrigation management on aquifer recharge is of paramount importance for this study area. To do so, an integrated water management perspective, whereby the multiple uses of surface water and groundwater resources are taken into consideration simultaneously, is necessary. Despite its strategic importance for drinking water supply, very few groundwater modeling studies have been carried out in the study area (e.g., Piccinini et al., 2017), none of them considering the interactions between surface and subsurface water from an integrated and physics-based point of view.

To this end, integrated surface-subsurface hydrological models (ISSHMs) (e.g., Paniconi and Putti, 2015; Fatichi et al., 2016) seem to be particularly well-suited, thanks to their capability of simulating the coupled surface and groundwater compartments of the

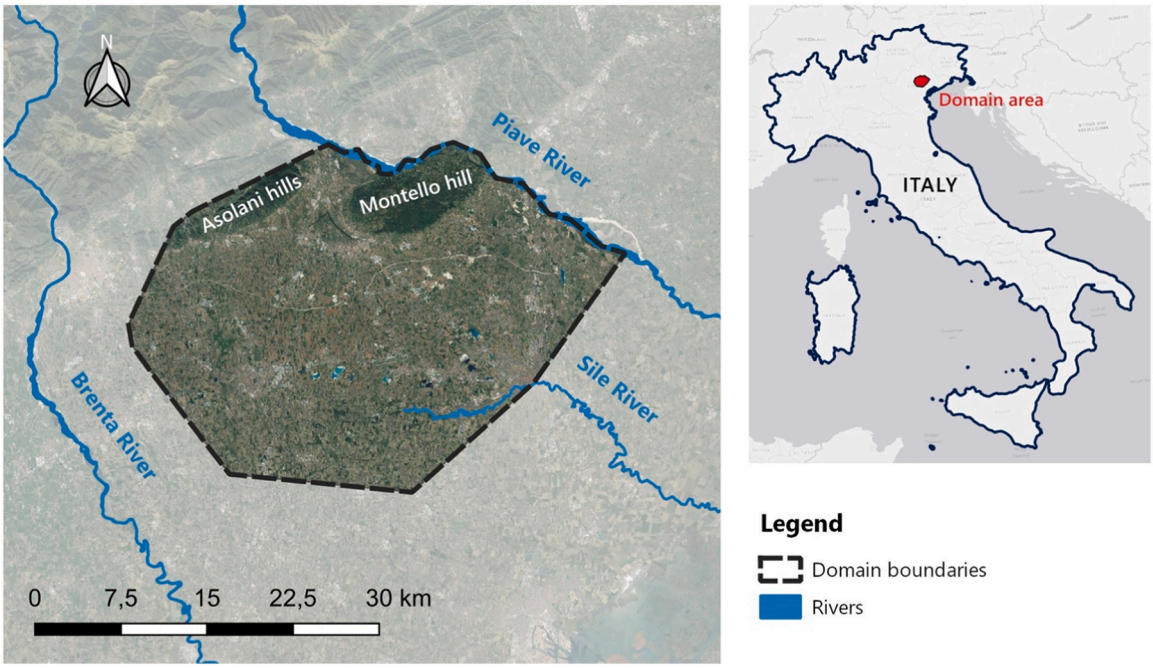

Fig. 1. Study area and its location in the Italian peninsula.

hydrological cycle. Some examples of state-of-the-art ISSHMs include the Process-Based Adaptive Watershed Simulator (PAWS; Shen and Phanikumar, 2010), CATchment HYdrology (*CATHY;* Camporese et al., 2010), HydroGeoSphere (HGS; Brunner and Simmons, 2012), MIKE SHE (Long et al., 2015), and ParFlow (Maxwell et al., 2015). ISSHMs have rarely been used as practical-operational decision support tools, having mainly been employed to reproduce experimental data (Pertti et al., 2017*;* Bizhanimanzar et al., 2019; Bizhanimanzar et al., 2020), to assess possible future scenarios of land use change (Azarnivand et al., 2020*;* Hossein and Kaveh, 2022), and to simulate contaminant spreading (Reszler and Fank, 2016*;* Gatel et al., 2019*;* Gatel et al., 2020), but generally stopping after the validation phase. Very few studies used ISSHMs to operationally support sustainable water resources management: Haque et al. (2021) presented an application of HydroGeoSphere to a Canadian groundwater system to investigate the impacts caused by water use, different withdrawal scenarios, and climate changes, while Surinaidu (2022) investigated the stream flow and groundwater response of an Indian river basin that supplies water to millions of people, subjected to rapid urbanization and increased agricultural pressures.

The main objective of this work was to develop an integrated surface–subsurface hydrological model of a groundwater system in the Venetian high plain, heavily exploited for drinking water supply, using the CATHY (CATchment Hydrology) model. After calibration and validation, the model was used to quantify current aquifer recharge and its possible evolution in response to changes in the irrigation management.

2. Material and methods

2.1. Study area

The study area (Fig. 1) is located in the Veneto region, northeastern Italy, and mainly comprises the Venetian plain between the Brenta and Piave Rivers. More specifically, the computational domain is delimited to the northeast by the Piave River, to the west by a flowline approximately parallel to the Brenta River, to the south by the *risorgive (*also known as *fontanili)* belt – a characteristic zone of groundwater resurgence – and to the North by the Montello and Asolani hills. Its extension is 891 km^2 and it represents a groundwater hydrosystem of particular relevance for drinking water supply in the Treviso province.

The main hydrogeological structure of the Venetian alluvial plain is known since the '70s, thanks to detailed studies by the *Consiglio Nazionale delle Ricerche* (CNR) (IRSA-CNR, Gruppo di studio sulle falde acquifere profonde della pianura Padana, 1976*)*. It can be subdivided in three main zones:

1. the high plain, also called *piedmont zone*, close to the mountains in the northwest of the region;
2. the middle plain, also called *risorgive* belt, between the high and the low plain;
3. the low plain, nearby the sea.

The subsurface material from the piedmont zone to the *risorgive* belt, the most relevant area for this study, is mainly formed by granular material (gravel and sand), which hosts an unconfined aquifer of variable thickness that flows from northwest to southeast with a mean velocity of a few meters per day order of magnitude.

A comprehensive knowledge of this hydrosystem is extremely important for an efficient management of the groundwater resources, which are used by several water utility companies located in the study area. These companies provided all the borehole data used in

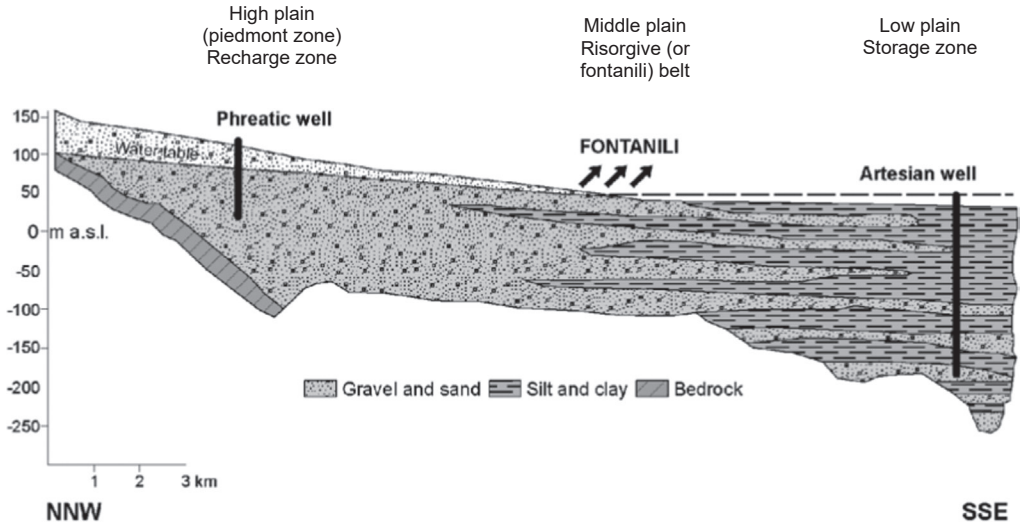

Fig. 2. Main hydrogeological structure of the Venetian plain. Adapted from Piccinini et al. (2017)

.

this study and described below (water levels, pumping rates when relevant, location of the wells, screening elevation, etc.).

2.2. The CATHY model

The integrated surface-subsurface hydrological model CATHY (Camporese et al., 2010; Scudeler et al., 2016; Weill et al., 2011) combines a three-dimensional finite element solver of the Richards' equation for variably saturated porous media and a one-dimensional finite difference solver of the diffusive wave approximation of the shallow water equations. In addition, CATHY can simulate coupled problems of solute transport in the surface-subsurface continuum by solving a three-dimensional advection-dispersion-reaction equation for the subsurface and a one-dimensional advection-diffusion equation for the surface (Weill et al., 2011; Gatel et al., 2019; Gatto et al., 2021).

Only a brief overview of the CATHY features more relevant to this research is given here, whereas more details can be found in Camporese et al. (2010).

Coupling between the surface and subsurface modules relies on a bo*undary condition-switching* procedure, which is based on two thresholds of soil water pressure head, a minimum ponding head, h_{min}, for the partitioning of rainfall into infiltration and surface runoff and a minimum pressure head, ψ_{min}, to distinguish between atmosphere-controlled and soil-limited evapotranspiration (Camporese et al., 2014). The latter, in particular, allows for a simple calculation of actual evapotranspiration from potential evapotranspiration, but is only valid for shallow rooted vegetation (Camporese et al., 2015).

Another method, based on the root water uptake approach by Feddes, is used here to compute actual evapotranspiration in CATHY. The water removed from the soil by the vegetation roots is represented as a sink term, which depends on the potential evapotranspiration, water content and root depth and density (Muma et al., 2013). The root density $\beta(z)$ is distributed along the depth as:

$$\beta(z) = \left[1 - \frac{z}{z_m}\right] e^{-\frac{p_z}{z_m} z} \quad (1)$$

where z is depth (i.e., positive downward), z_m is the maximum rooting depth, and p_z is an empirical parameter (Camporese et al., 2015). The effect of water stress is modeled through the multiplication of the potential root water uptake by the Feddes reduction function (Feddes et al., 1976). The Feddes reduction function is a piecewise linear function that describes a root water uptake reduction factor that goes from 0 to 1 as a function of pressure head ψ. Five stages of water uptake are bounded by four pressure head thresholds ($\psi_s > \psi_{an} > \psi_d > \psi_{wp}$). The reduction function is zero above saturation, ψ_s, a phase of complete lack of oxygen and null water uptake (anoxic phase). By decreasing the value of pressure head between ψ_s and ψ_{an}, the root water uptake increases linearly as air-filled porosity increases. In the range between ψ_{an} and ψ_d (constant rate phase), there is no water stress or oxygen stress and the root water uptake equals the potential root water uptake. Between ψ_d and ψ_{wp} (falling rate phase), water uptake decreases linearly to zero. Below ψ_{wp}, delimiting the permanent wilting phase, the root water uptake equals zero (Camporese et al., 2015; de Melo and de Jong van Lier, 2021).

Nonlinearities in the Richards equation arise from the soil water retention curve, which in CATHY is modeled through the van Genuchten (1980) equation:

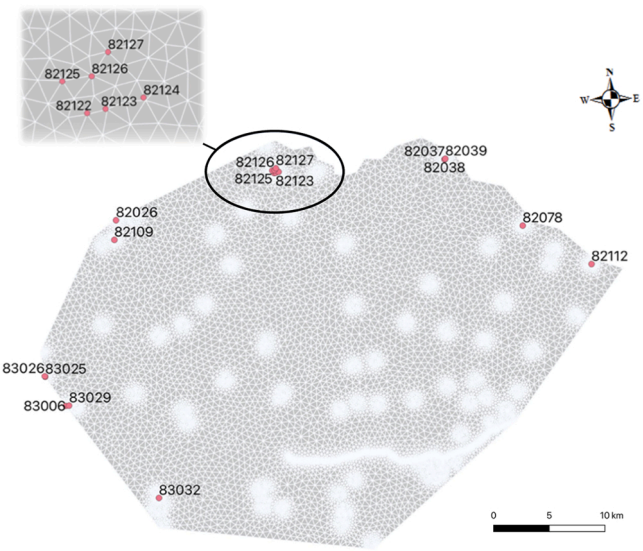

Fig. 3. Location of active pumping wells within the computational mesh. Mesh refinement is visible in correspondence of the Sile River and observation wells.

$$\theta = \theta_r + \frac{\theta_s - \theta_r}{[1 + |\alpha \quad \psi|^n]^m} \tag{2}$$

where θ is the soil water content ($m^3 \cdot m^{-3}$), θ_r is the soil residual water content ($m^3 \cdot m^{-3}$), θ_s is the porosity (or soil saturated water content) ($m^3 \cdot m^{-3}$), ψ is pressure head (m), α is a scale parameter inversely proportional to the mean pore diameter (m^{-1}), n and m are the shape parameters of soil water characteristics with $m = (1 - 1/n)$.

In this study, as the focus is on quantifying groundwater recharge, solute transport is not simulated. In addition, to save computational time, the surface module is not activated. This means that the partitioning of rainfall and/or irrigation into overland flow and infiltration is still computed by the model through the boundary condition-switching procedure described above. However, overland flow is not routed along the channel networks or hillslopes, but it is instantly removed from the computational domain. This allowed us to considerably decrease the computational effort, while still computing recharge as an internal flux and not as an input to the model, contrary to standard groundwater models solving the saturated zone only.

2.3. Model setup

2.3.1. Mesh

The computational mesh was built starting from a triangular finite element mesh with 16,112 nodes (Fig. 3), replicated vertically into 14 node slices, for a total number of 225568 nodes. Initially, each layer was a parallel replica of the surface. Later, the bottom topography was calibrated as reported in Section 2.4.1 to allow for a spatially variable aquifer thickness. The Sile River, in the southeastern part of the domain, indicates approximately the beginning of the *risorgive* belt and has been discretized with finer triangles, as well as all the locations corresponding to observation and/or pumping wells (Fig. 3).

2.3.2. Non atmospheric boundary conditions and initial conditions

Active pumping wells have been represented in the model through sink terms, numerically equivalent to Neumann boundary conditions, extracting water from nodes corresponding to their screening location. Time-variable pumping rate and water table data were provided by the water utility companies operating in the study area (Trentin, 2021) and are available from April 15th 2018 to August 31st 2020. Pumping rates vary from well to well, ranging between 2.0×10^{-6} m^3 s^{-1} and 4.3×10^{-2} m^3 s^{-1}. Fig. 3 reports the position of the active wells within the computational mesh. Note that, as the computational domain only considers the unconfined aquifer, pumping wells withdrawing from underlying confined aquifers were not included in the model.

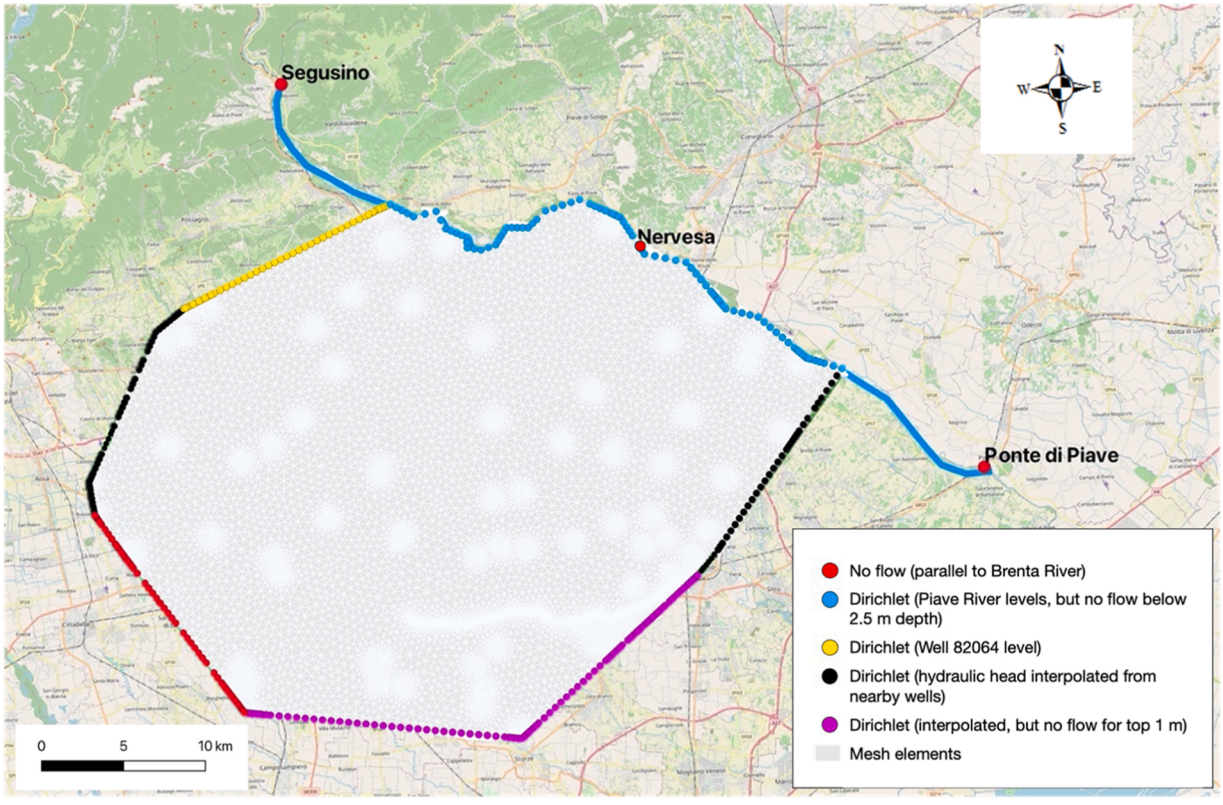

Fig. 4. Domain boundary conditions.

Boundary conditions vary along the perimeter of the domain and its depth. To the northeast, along the boundary defined by the Piave River (cyan boundary in Fig. 4), a Dirichlet boundary condition was imposed, with pressure head values computed according to the time series of river water level data. These were evaluated by spatio-temporally interpolating the available time series in three observation stations along the river, namely Segusino, Nervesa and Ponte di Piave (https://wwwold.arpa.veneto.it/bollettini/storico/Mappa_2018_LIVIDRO.htm?t = RG). This Dirichlet boundary condition was imposed until a depth of 2.5 m (an average, reasonably assumed, vertical distance from the top of the banks to the river thalweg), while a no flow boundary condition was imposed below, due to symmetry. In the northwestern boundary (yellow in Fig. 4), pressure head values consistent with the water level time series in well 82064 were imposed. In the southwestern part (red in Fig. 4), the domain is approximately parallel to the Brenta River, which flows a few kilometers away; therefore, no flow conditions were reasonably assumed. To the southeast and to the west (black in Fig. 4), Dirichlet boundary conditions were imposed, with pressure head values obtained through a Kriging interpolation starting from data available in nearby observation wells (Trentin, 2021). Analogous Dirichlet boundary conditions were imposed to the south (magenta in Fig. 4), except for the three shallow layers, in which a no flow condition was imposed, due to the presence of a lower conductivity soil in the *risorgive* area.

The initial conditions were generated through preliminary steady-state simulations with the same boundary conditions (but time-averaged) as described above. The steady-state pressure head distribution was then imposed on the domain as plausible initial conditions.

2.3.3. Land use

The land use distribution, sourced from the *Carta di copertura del suolo* (land use map) of the Veneto Region geoportal (https://idt2.regione.veneto.it/idt/downloader/download), was used to assign spatially variable Feddes parameters to the computational mesh. For ease of implementation, the original 34 land use classes in the map were aggregated into six macro-classes with similar characteristics (Table 1).

Fig. 5 reports the spatial distribution of the six macro-classes within the computational domain. The more widespread land uses are arable land (42 %) and urban centers (29 %). These data exemplify how the economic Venetian traditions are strongly linked to agriculture, but also highlight a worrying trend of decrease in working agricultural area, in favor of increasing urban and industrial areas (ARPAV, 2022). Each land use macro-class is associated to a different rooting depth (z_m), as reported in Table 1, while the Feddes function pressure head thresholds are considered uniform in space. In particular, oxygen stress was not considered in the simulations and the only relevant parameter values are $\psi_d = -0.4$ m and $\psi_{wp} = -150$ m (Feddes et al., 1976).

2.3.4. Atmospheric boundary conditions

Atmospheric boundary conditions were assumed variable in space and time (with a daily resolution) and consist of the net precipitation (i.e., rainfall minus potential evapotranspiration) plus irrigation. Precipitation daily data were obtained from the ARPAV website (https://wwwold.arpa.veneto.it/bollettini/storico/Mappa_2018_PREC.htm?t = RG) and spatially interpolated (Trentin, 2021), while irrigation rates were provided by Consorzio di Bonifica Piave and applied on the relevant areas. The FAO56 Penman–Monteith formula was used to estimate the potential crop evapotranspiration (ET_c), based on the reference evapotranspiration (ET_o) and a crop coefficient (K_c) related to the vegetation types and period of the year (Allen et al., 2006):

$$ET_c = K_c \quad ET_o,$$

Where units of ET_c and ET_o are mm d^{-1} and K_c is dimensionless.

Fig. 6 shows an example of atmospheric boundary flux distribution in a 2018 rainy winter day. On average, the net precipitation tends to be larger in high-terrain areas, where rainfall is usually more intense and lower temperatures reduce evapotranspiration (Barbi et al., 2011).

2.3.5. Soil surface heterogeneity

According to the *Soil map of the Veneto Region* (*https://gaia.arpa.veneto.it/maps/294*), the 1 m-thick topsoil of the computational domain has been subdivided in four hydraulic conductivity macro-areas. Each macro-area is characterized by a qualitative indication of the saturated hydraulic conductivity (K_s) range of variability:

1. low = $1.0 \times 10^{-8} - 1.0 \times 10^{-7}$ m s^{-1};
2. moderately low = $1.0 \times 10^{-7} - 1.0 \times 10^{-6}$ m s^{-1};

Table 1
Land use macro-classes and corresponding rooting depths.

Macro-Classes	Legend	Root depth (m)
1	Urban center	0.1
2	Arable land	0.5
3	Orchards	5.0
4	Gardens	0.5
5	Deciduous forest	10
6	Wet fluvial environments	0.1

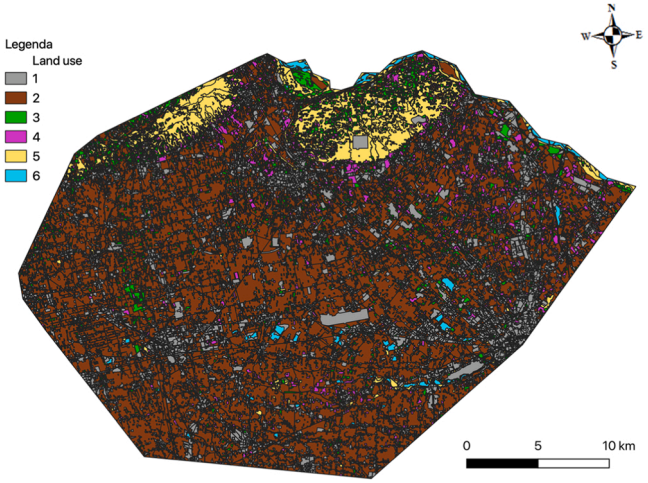

Fig. 5. Land use in the study area (the description of each class is reported in Table 1).

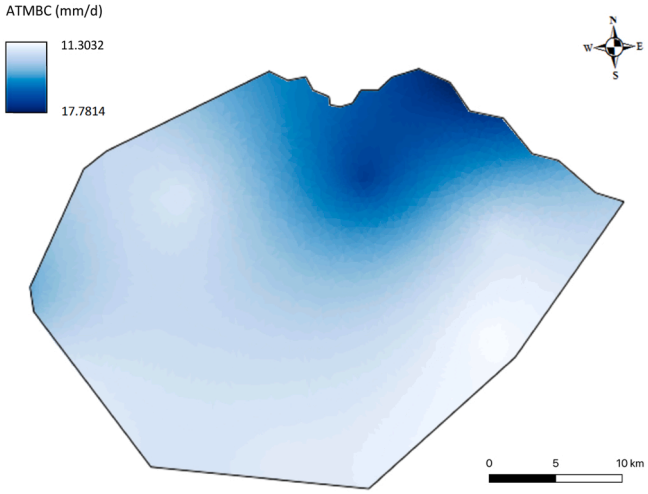

Fig. 6. Example of atmospheric boundary conditions (ATMBC) distribution (mm d^{-1}).

3. moderately high = $1.0 \times 10^{-6} - 1.0 \times 10^{-5}$ m s^{-1};
4. high = $1.0 \times 10^{-5} - 1.0 \times 10^{-4}$ m s^{-1}.

These four areas have been complemented by a "South of Sile" zone, where stratigraphic evidence suggests a moderately low hydraulic conductivity, and an aquifer zone, below the topsoil (Trentin, 2021). Fig. 7 shows the resulting hydraulic conductivity map in the computational domain. The northeast part is characterized by a zone of high K_s (green). A low K_s strip (blue) approximately delimits the *risorgive* belt. In correspondence with the Montello and Asolani hills to the north, and south of Sile, K_s is in the low to moderately low range (yellow and magenta). Moderately high K_s (orange) characterizes the rest of the surface, while the aquifer (black) occupies the deeper layers.

Initially, the mid values of K_s in the above ranges were set for the simulations. Then, these values were tuned as described in Section 2.4. Next, the high and moderately high K_s zones were aggregated into the "aquifer" zone, whose spatially variable hydraulic conductivity was calibrated as also reported in Section 2.4. Specific storage was assumed constant and equal to 10^{-3} m^{-1}, while the parameters of the capillary retention curves (Eq. 2) and relative hydraulic conductivity curves (van Genuchten, 1980) for the different soils were obtained from Carsel and Parrish (1988).

2.4. Model calibration

2.4.1. Aquifer bottom and average aquifer K_s

In the first calibration step, the aquifer bottom and average hydraulic conductivity of the aquifer formation were calibrated with

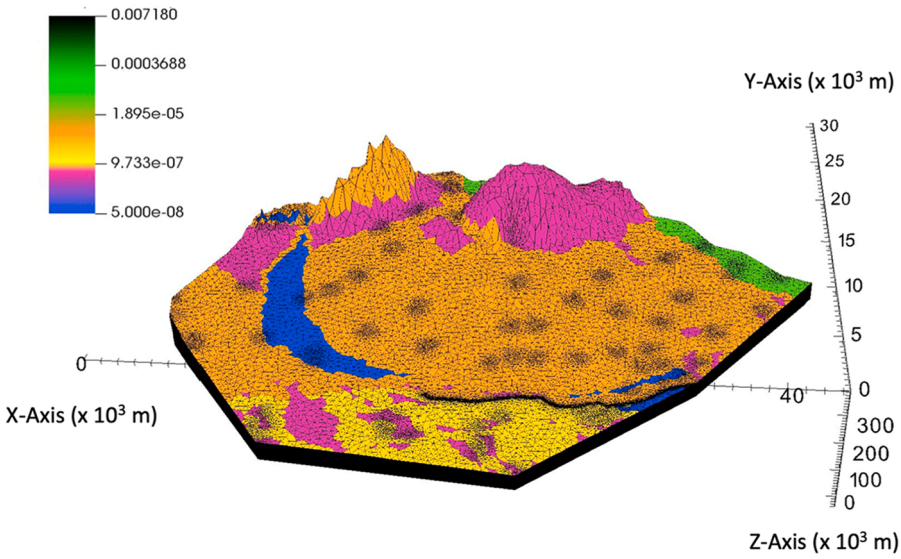

Fig. 7. Hydraulic conductivity zones of the study area. Aquifer (black), high Ks (green), moderately high Ks (orange), South of Sile river (yellow), moderately low Ks (magenta), low Ks (blue). The colorbar indicates hydraulic conductivity in m s^{-1}.

FePEST, the FeFlow-integrated extension for PEST. To the best of our knowledge, aquifer bottom calibration is not a common step in groundwater modeling. This would not be necessary in cases where a detailed characterization of the bottom is available (e.g., Camporese et al., 2019); however, this rarely happens. More typically, when no detailed information is available on the topmost aquitard or bedrock, as in our study area, the bottom of the aquifer is assumed to be flat or parallel to the land surface (e.g., Maxwell et al., 2015). This, in the present study, would result in an unrealistic and not credible configuration. Currently, CATHY lacks the capability to calibrate the aquifer bottom and its implementation would have been too time-consuming. FeFlow is a finite-element subsurface flow and transport modeling system with functionalities that go from variably saturated flow to variable fluid density mass and heat transport, up to multispecies reactive transport, accessible via a comprehensive user interface (Diersch, 2013). PEST (Parameter ESTimation) is a widespread non-linear inverse modeling code (Doherty, 2015) especially used in decision support and environmental decision making for groundwater modeling. Through a Gauss-Levenberg-Marquardt algorithm (Doherty, 2015), PEST searches for the set of model parameters that minimizes the objective function:

$$\varphi = \sum (w_i r_i)^2,$$

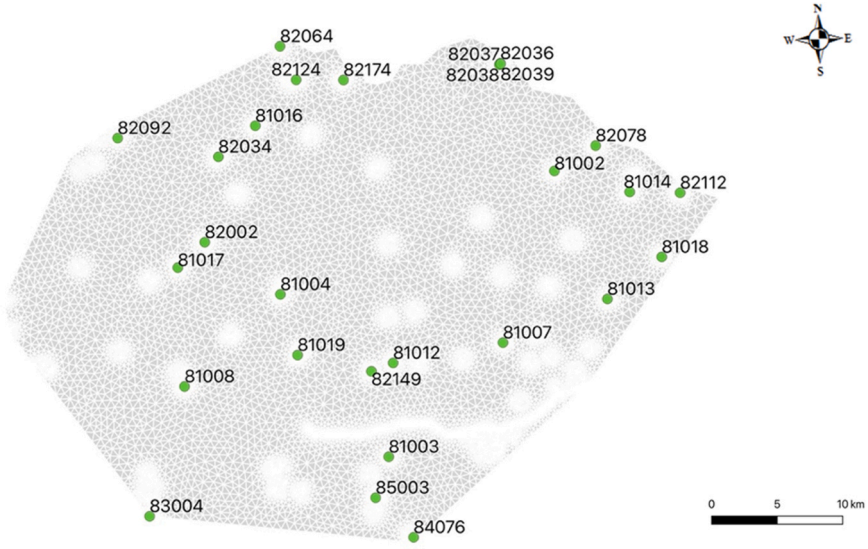

Fig. 8. Location of the observation wells used in the model calibration. The wells located along the boundaries (82064 and 83004) were used for the boundary conditions and therefore excluded from the calibration procedure.

where r_i, the residuals, are here defined as $r_i = h_{calculated} - h_{observed}$, with h calculated and observed hydraulic heads, while w_i are weights applied to the residuals. The 28 available observation wells, out of which 26 were used for the calibration, are reported in Fig. 8. In these wells, water table time series are available for the period that goes from mid-April 2018 to the end of August 2020.

The first bottom calibration using FePEST was performed with the following model configuration:

1. 2D steady-state model in non-irrigation period (i.e., the average atmospheric flux consisted of rainfall minus potential evapotranspiration, with time-averaged boundary conditions and equally time-averaged water table levels in the objective function);
2. homogeneous aquifer K_s equal to 1.0×10^{-3} m s^{-1};
3. minimum bottom elevation imposed at – 40 m a.s.l., based on available geological information.

A pilot points parameterization was employed, with 106 pilot points distributed all over the domain. The estimation of the continuous aquifer bottom elevation was performed using Ordinary Kriging and setting an isotropic exponential variogram with a range of 10^4 m. After the aquifer bottom, also the average aquifer K_s was calibrated, whereby the aquifer zone includes the high and moderately high surface zones as well as the computational layers below, for the entire extent of the study area.

2.4.2. Sensitivity analysis on soil surface K_s

After calibrating the aquifer bottom and average K_s, these pieces of information were transferred in CATHY. A sensitivity analysis was then performed by changing (one at a time) the K_s values of each surface zone within the ranges indicated by the soil map (Section 2.3.5), to find the combination that best matched the observations in transient conditions for the period between mid-April 2018 and mid-June 2019. The remaining data (until August 2020) were left for the model validation.

2.4.3. FePEST calibration of heterogeneous aquifer K_s

A further calibration step was performed with FePEST to obtain a heterogeneous K_s distribution for the aquifer formation, i.e., the entire domain except for the low and moderately low K_s zones. This calibration step was performed in steady-state conditions via pilot points parameterization. In the 3D mesh, with bottom elevation calibrated as previously described, the same spatial distribution of 106 pilot points was assigned to each one of the 13 element layers. The optimization algorithm was allowed to adjust the hydraulic conductivity values at the pilot points of one layer only, while the parameters on the remaining layers were tied to maintain vertical homogeneity. This setting was chosen to recreate a single numerical layer where more geometrical layers are present. Ordinary Kriging was used to estimate the continuous hydraulic conductivity field for each layer, based on the optimized values at the pilot points. Again, an isotropic exponential variogram with range 10^4 m was assumed.

2.4.4. SCE-UA fine tuning

The last step of the model calibration was performed in CATHY using the SCE-UA algorithm (Duan et al., 1994). This step was carried out to further improve the model performance and to consider transient conditions (also from mid-April 2018 to mid-June 2019) in the calibration. This was performed on six multiplicative parameters, α_i, for each of the soil conductivity classes from the previous FePest calibration. Note that a uniform multiplicative parameter was also considered for the heterogeneous aquifer formation. The parameters were allowed to vary from 0.2 to 5. An additional multiplicative parameter was considered for the anisotropy ratio $\alpha_{\mathrm{ANISOTROPY}}$, i.e., the ratio between vertical and horizontal hydraulic conductivity, which was allowed to vary from 0.1 to 1.

2.5. Model validation and future scenario of irrigation management

After the calibration, a validation run was performed using the remaining part of the data set from mid-June 2019 to the end of August 2020, immediately after the calibration period. This simulation was run using:

1. calibrated bottom,
2. final distribution of hydraulic conductivity from the SCE-UA fine-tuning procedure,
3. updated boundary conditions,
4. initial conditions of pressure head derived from the end of the calibration simulation,
5. the same 26 wells considered in the calibration for assessing the model validation performance.

Once the calibrated and validated model was obtained, it was possible to perform a simulation scenario with varied irrigation management. A large fraction of the study area is currently characterized by flood irrigation, which requires a large amount of water, in this case withdrawn from the Piave River. To comply with the new European and Italian legislation, a transition from flood irrigation to sprinkler irrigation is ongoing and planned to be completed in a few years.

To assess the quantitative impact that this planned irrigation method change will have on the groundwater recharge, we set up a simulation with reduced irrigation rates in the areas that will be affected by the irrigation method variation and corresponding increased water levels in the Piave River, whose rating curve in the monitoring station of Segusino (https://wwwold.arpa.veneto.it/bollettini/storico/2020/0327_2020_PORT.htm) is shown in Fig. 9.

Next, we quantified the expected difference in water withdrawals from the river based on irrigation data provided by the Consorzio di Bonifica Piave. Considering average irrigation rates during the irrigation season of 1.86 and 0.62 l s^{-1} ha^{-1} for flood irrigation and

sprinkler irrigation, respectively, and a total area affected by the variation equal to 25,000 ha, the resulting reduction of discharge derived from the Piave River is (1.86 – 0.62) l s^{-1} ha^{-1} × 25,000 ha = 31,000 l s^{-1} = 31 m^3 s^{-1}.

As a result, the average flow discharge in the Piave River should increase during the irrigation period by 31 m^3 s^{-1}, corresponding to an average water level increase of 0.2 m (Fig. 9). This was used to correct the northeast Dirichlet boundary conditions, while reduced atmospheric fluxes consistent with the decrease in irrigation were applied to the surface of the model domain.

Total groundwater recharge for this simulation scenario as well as the calibration simulation was calculated as in Gauthier et al. (2009), i.e., by considering at each time step the vertical component of Darcy fluxes across the water table when these are directed downward. Recharge outputs include both spatial maps at different times and the total cumulative recharge integrated in time and space.

3. Results

3.1. Uncalibrated model

The transient simulated heads in the observation wells are compared with the measurements in the scatter plot of Fig. 10 *a)* for the uncalibrated model, i.e., with prior aquifer bottom and hydraulic conductivity. The uncalibrated model results in head overestimation for more than half of the wells; furthermore, for about one third of them the simulated data are quite far from the observed data, with an overall RMSE of 27.02 m.

3.2. Calibrated simulations

The spatial distribution of the aquifer bottom resulting from the FePEST calibration is shown in Fig. 11 *a)*. Consistent with available, albeit qualitative, geological information the aquifer bottom tends to increase while going from south to north, i.e., from the lowest elevations toward the high plain and the piedmont zone. Between the *risorgive* belt and the southern boundary, the elevation of the bottom is constrained to the –40 m a.s.l. bound, the average estimated elevation for the top of the shallowest aquitard.

The average aquifer K_s value obtained from the homogeneous calibration (7.18 ×10^{-3} m/s) is larger than the prior value (1.0 ×10^{-4} m/s). After the new aquifer bottom and average K_s value were implemented in CATHY, the sensitivity analysis on the hydraulic conductivity values of the surface soils gave the results reported in Table 2, where the column denoted with "Best" contains the combination of parameters for which the RMSE between observed and measured heads is the smallest.

This allowed for a slight improvement in the simulated water table level, but not still satisfactory (not shown).

The subsequent calibration step, performed with FePEST and fine-tuned with SCE-UA, resulted in the heterogeneous distribution of K_s shown in Fig. 11 *b) and c),* while Table 3 reports the calibrated multiplicative parameters obtained with SCE-UA. In the first three layers of the computational domain, corresponding approximatively to the topmost 1 m-thick soil, the areas of low and moderately low K_s were kept as in the ARPAV soil map, with the values indicated in Table 2, under the column *Best*, while the whole aquifer zone is now characterized by a marked heterogeneity. Red areas indicate zones with high conductivity, mainly in the southeast of the domain, green areas have an intermediate conductivity in the order of magnitude of 1.0 × 10^{-5} m s^{-1}, while light blue areas, mainly in the northern part of the domain, close to the Montello and Asolani hills, indicate lower conductivity soils.

Fig. 10*b)* shows the scatter plot of the final calibrated simulation in which the heterogeneous bottom and hydraulic conductivity

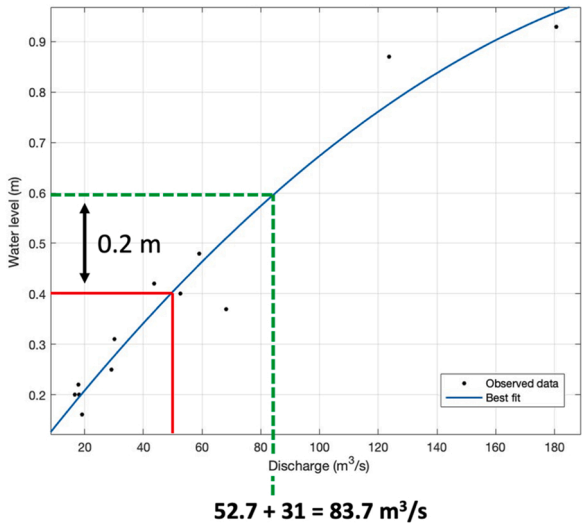

Fig. 9. Rating curve of the Piave River at Segusino in June, with indication of expected increased discharge and water levels resulting from reduced withdrawals for irrigation.

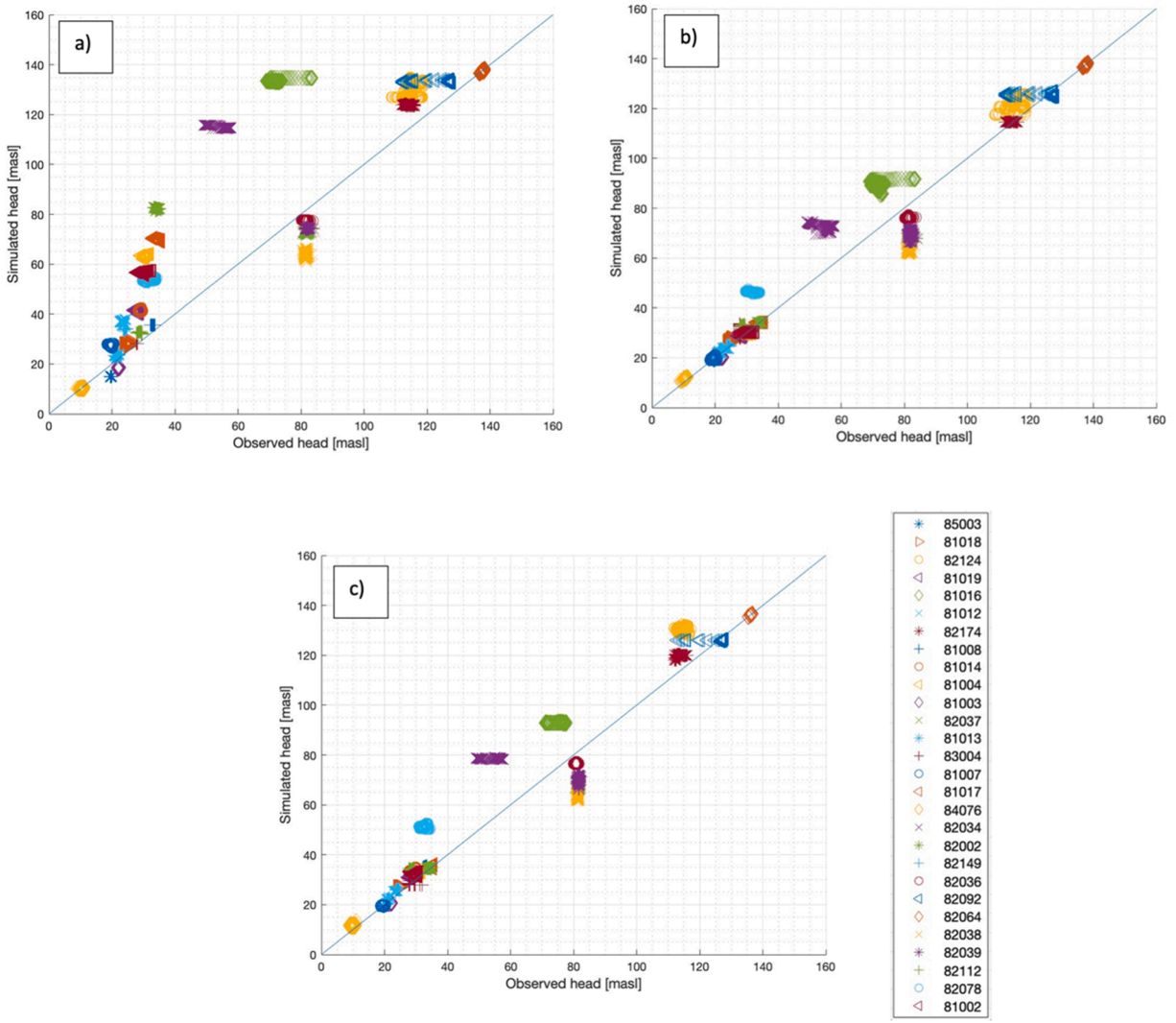

Fig. 10. a) Scatter plot of observed vs simulated hydraulic head for a) the uncalibrated model (RMSE = 27.02 m), b) the final calibrated model (RMSE = 7.78 m), and c) the validation step (RMSE = 9.38 m).

field obtained through the SCE-UA have been implemented. Compared to the uncalibrated simulation, we can observe a strong improvement in the results. Some of the wells still exhibit a slight under or overestimation, but the overall RMSE value is now 7.78 m, i.e., less than one third of the uncalibrated RMSE. An area close to the Piave River in the northeast part of the domain, in particular, is the one where the mismatch between observed and simulated data is particularly large (wells 82036, 82037, 82038 and 82039). This may be attributed to the uncertainty in the shape of the aquifer bottom.

The same model configuration was used for the validation simulation, over the period June 2019 -August 2020. The results shown in Fig. 10 *c)*, present a slight increase of RMSE (9.38 m).

3.3. Irrigation variation scenario

Figure 12 highlights the differences in water table levels for the five wells most affected by the irrigation method variation. The location of these wells is highlighted in Fig. 12*f*, along with the current spatial distribution of sprinkler (blue) and flood (red) irrigation regions in the study area. Observed water table is reported in red, while black and green indicate the simulation results with sprinkler and flood irrigation versus sprinkler only irrigation, respectively. These five observation wells, all located within the region affected by the irrigation management change, show a marked decrease of water table during the irrigation season compared to the reference simulation. Water table levels in observation wells 81003 and 81019, at the west border and south of the current flood irrigation area, respectively, were also affected (not shown), but much less than the other five.

The total cumulative recharge calculated by CATHY in the two simulations is shown in Fig. 13 and highlights that the recharge in

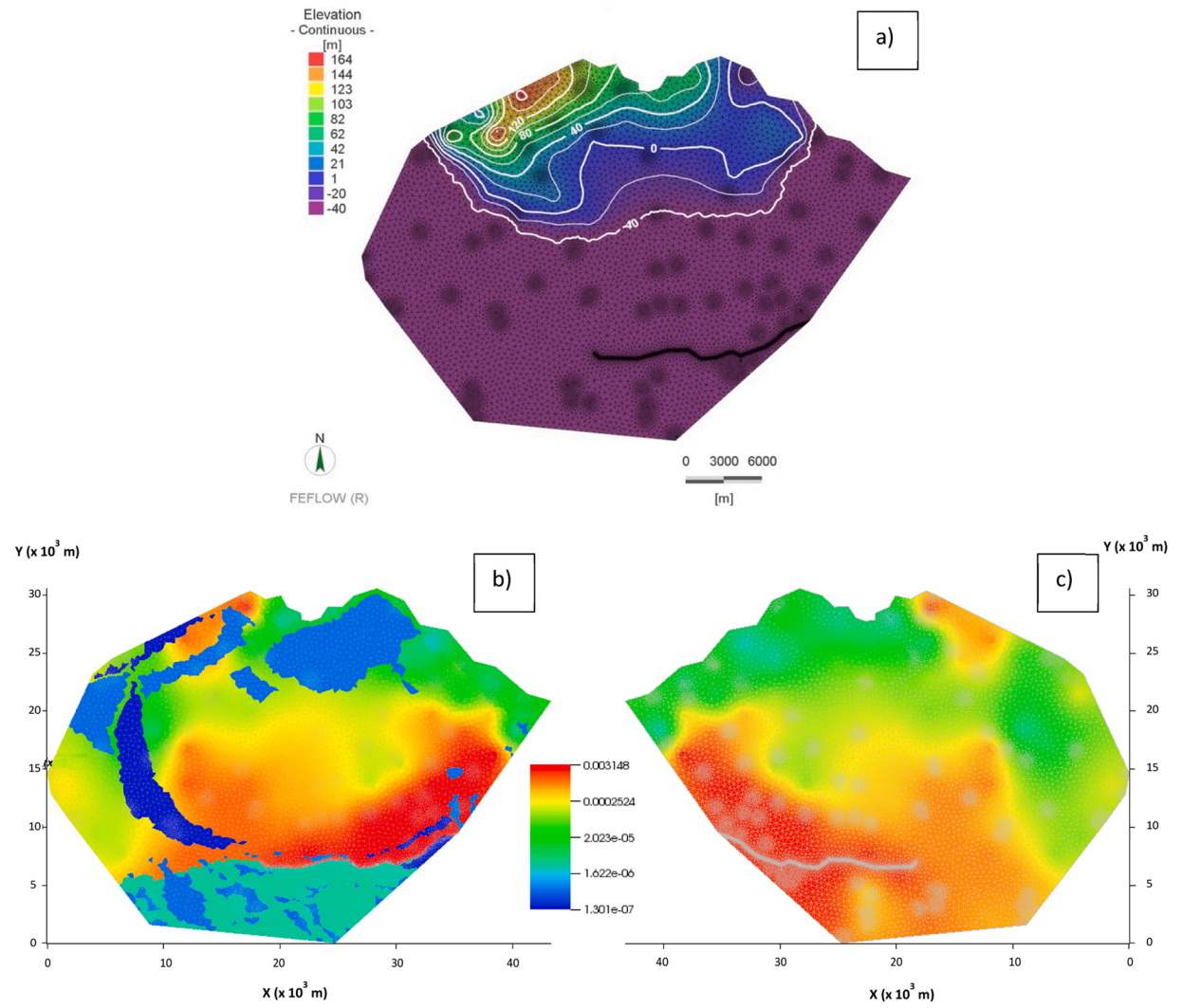

Fig. 11. a) Calibrated bottom elevation. Top (b) and bottom (c) view of the hydraulic conductivity distribution in the computational domain. The view from the bottom highlights the heterogeneous K_s distribution within the aquifer.

Table 2
Hydraulic conductivity values used in the sensitivity analysis on the surface soil zones. Colors in the first column are consistent with those reported in Fig. 7 for the various soil formations.

Hydraulic conductivity	Base ($m\ s^{-1}$)	Minimum ($m\ s^{-1}$)	Maximum ($m\ s^{-1}$)	Best ($m\ s^{-1}$)
Aquifer	1.00E-04	-	-	7.18E-03
Moderately high	5.00E-06	1.00E-06	1.00E-05	1.00E-05
South of Sile River	5.00E-06	1.00E-06	1.00E-05	1.00E-06
Low	5.00E-08	1.00E-08	1.00E-07	5.00E-08
Moderately low	5.00E-07	1.00E-07	1.00E-06	1.00E-07
High	5.00E-05	1.00E-05	1.00E-04	1.00E-04

Table 3
Multiplicative parameters calibrated with SCE-UA.

α_1	α_2	α_3	α_4	α_5	α_6	$\alpha_{ANISOTROPY}$
1.73	3.15	3.14	2.60	4.29	2.18	0.24

the scenario with sprinkler only irrigation (398 mm) is about 10 % less compared to the current scenario (446 mm). Further insights about this important, yet preliminary, result can be gained by the spatial map of the recharge averaged in time over the irrigation season (Fig. 14*a*) and its difference between the two scenarios (Fig. 14*b*). From the latter, in particular, we can observe how the spatial contribution of the irrigation management change is relatively limited within the entire study area. Also, by comparing the areas characterized by higher recharge differences with Fig. 11 *b)* and *c)*, it seems that a combination of high K_s and irrigation transition is required to result in a significant impact, while irrigation transition alone is not sufficient. The unrealistically high values of recharge to the north of the domain are most likely due to numerical artifacts associated to the boundary conditions. These artifacts are extremely localized and do not affect the total recharge estimate.

4. Discussion and conclusions

We calibrated and validated an integrated surface-subsurface hydrological model for the Venetian plain between the Piave and Brenta Rivers, with the main objective of estimating current recharge fluxes into the unconfined aquifer and assessing the possible impacts of changing the irrigation technique from flood irrigation to sprinkler irrigation, currently ongoing to fulfil recent European directive requirements.

Calibrating the bottom of the computational domain and the hydraulic conductivity distribution resulted in a model setup that can reasonably and satisfactorily reproduce the observed water table in 26 observation wells scattered within the study area. Having confidence that the model gives plausible predictions, we computed the spatio-temporally variable recharge over the study area and its cumulative values for the current situation and a scenario where flood irrigation is fully replaced by sprinkler irrigation.

The current recharge, here defined exclusively as the vertical downward flux reaching the water table and derived mainly from rainfall and excess irrigation, was estimated in about 450 mm for a 14-month simulation. This is much less than previous estimates reported in the literature. Fabbri et al. (2016), for instance, suggested more than 1200 mm/year (rainfall plus irrigation contribution) for a very similar study area. However, their estimate is for soil surface infiltration and derived from a water balance based on input and output fluxes evaluated with data collected within the period 1996–2007. Even though infiltration is typically larger than recharge and climatic conditions have changed since then, these factors are likely not sufficient to explain the large difference between their estimate and the recharge value computed here by CATHY. Considering not only the (sometimes) poor reliability affecting their data (as acknowledged by the above Authors in their study) but also the uncertainties in our model (e.g., boundary conditions, initial conditions, stratigraphical information, parameterization, etc.), further studies are recommended to achieve a consensus on the quantification of recharge, which represents a term of paramount importance for the water balance and the sustainable management of water resources in the study area.

Despite all the uncertainties, the model simulates the observed water table dynamics with a relatively small error, compared to the size of the computational domain. Indeed, if we normalize the root mean square errors with respect to the difference between the highest and the lowest value of the observed water level (i.e., 138.3–8.8 = 129.5 m), the resulting normalized root mean square errors are 6 % and 7.25 %, for the calibration and validation, respectively.

For this reason, we believe that the simulated difference between current recharge and the one under a future scenario of changed irrigation technique is still meaningful. In particular, our simulations show that aquifer recharge in the study area should be affected by the transition from flood irrigation to sprinkler irrigation less considerably than expected, with an estimated decrease of about 10 % against a reduction of water withdrawn from the Piave river equal to 50 %. This relatively limited impact, at least in the short term, can be explained by two main factors. First, the spatial map of the mean recharge over the irrigation season shows that overall recharge seems to be more controlled by the hydraulic conductivity distribution than by the irrigation method. Second, the area affected by the change in irrigation techniques is less than 30 % of the computational domain; therefore, a more localized study focused entirely on this area would likely result in a more significant impact. In fact, in the wells directly affected by the recharge decrease, the model estimated an average reduction (Δh) of the mean water level of approximately 0.5 m. At first thought, it may seem not significant. However, a back-of-the-envelope calculation reveals that it would correspond to a yearly increase in energy spent for pumping equal to $\gamma Q \Delta h T = 9806 \times 0.01 \times 0.5 \times 8760 = 430$ kWh/well (where γ is the specific weight of water, Q is a typical daily pumping rate close to the area mainly affected by the recharge decrease, and T is the number of hours in a year), likely resulting not only in increased costs for the water utility companies (and hence for the users) but also in increased CO_2 emissions.

Overall, the results of this study, albeit relevant, should be considered as preliminary. To corroborate them, we need to improve the model calibration and validate the resulting parameterization against additional (and currently lacking) large-scale information about the structure and heterogeneity of the subsurface in the area of interest. Airborne electromagnetic surveys, currently being planned by a consortium of water utility companies in the area, complemented by ground-based stratigraphic investigations and data re-analyses could provide much needed data toward this goal. In particular, a large stratigraphical database, recently collected, is undergoing a process of filtering and homogenization and will provide, subject to advanced geostatistical analyses, a robust comparison with the distribution of the aquifer bottom found in this study through model calibration.

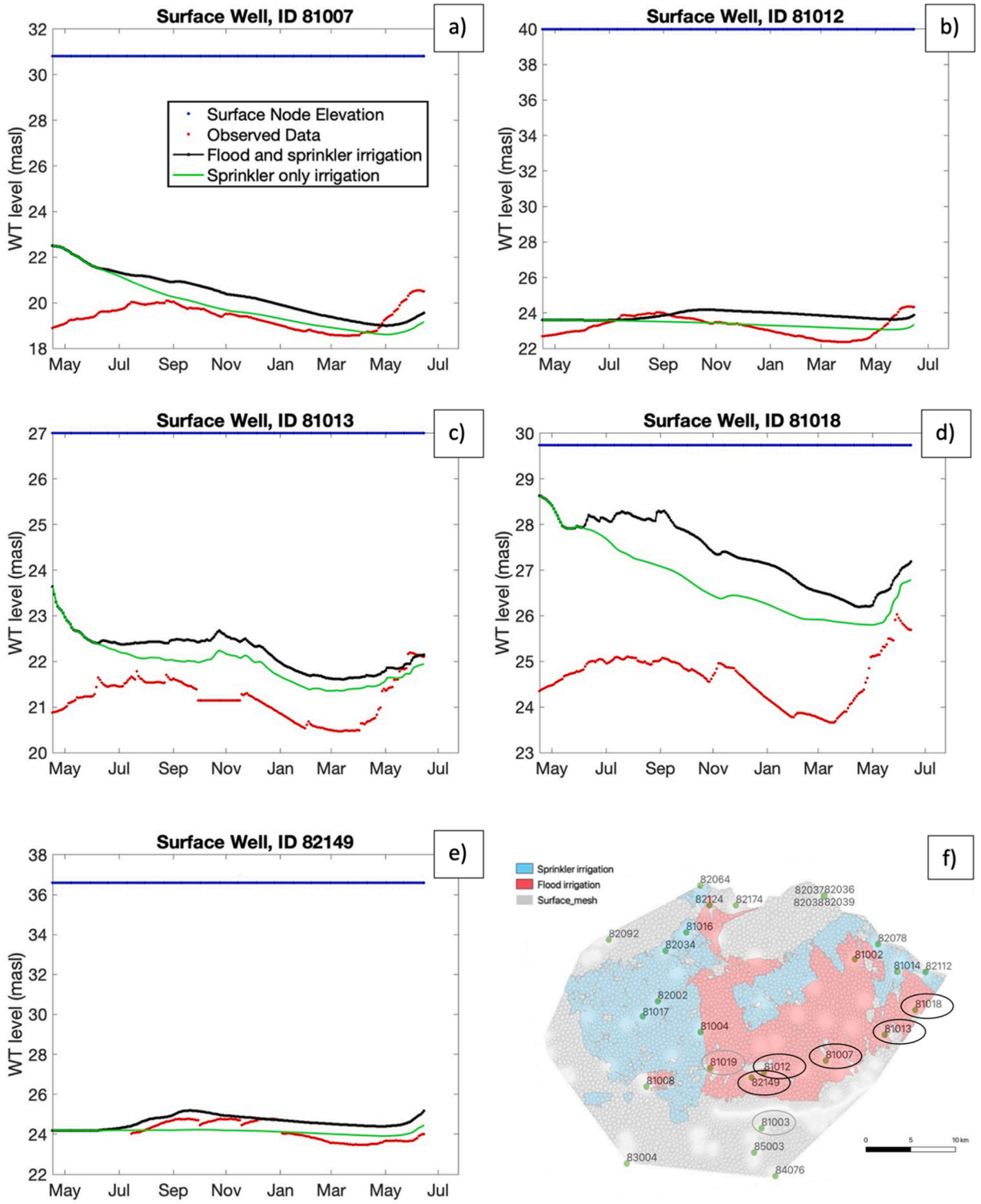

Fig. 12. (a to e) Water table (WT) levels simulated in the changed irrigation scenario compared to the reference simulation and observations, in the group of wells indicated in f).

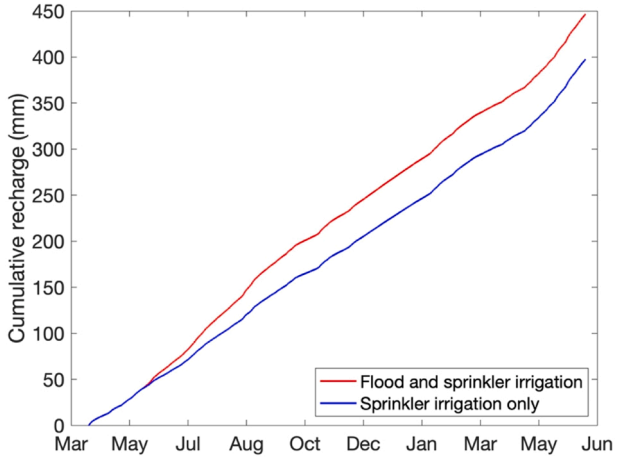

Fig. 13. Total cumulative recharge (mm) in the two irrigation scenarios.

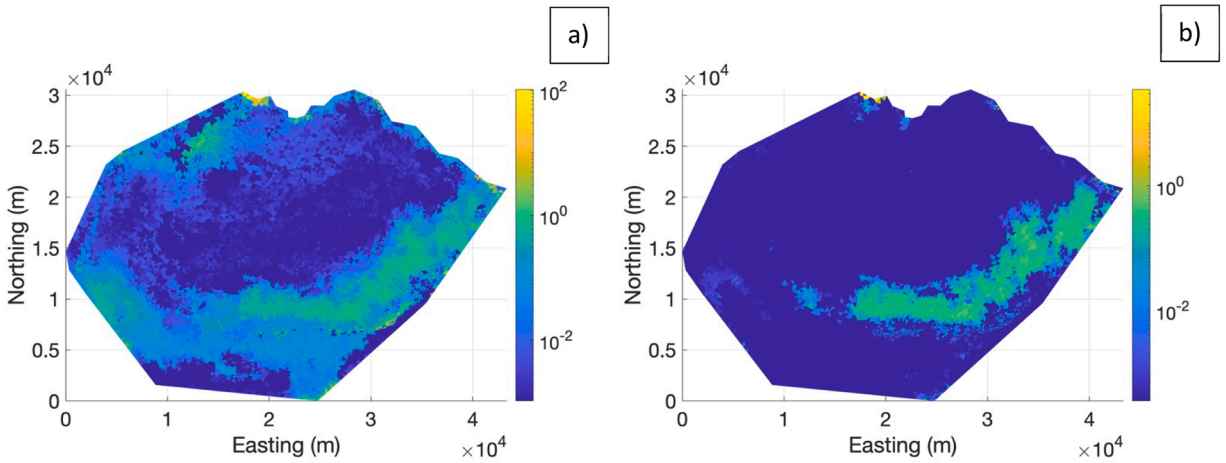

Fig. 14. a) Mean spatial recharge [l/s ha] simulated over the irrigation season 2018/05/31–2018/08/31 and b) difference between the mean spatial recharge of the current irrigation scenario (flood and sprinkler) and the future scenario (sprinkler only).

CRediT authorship contribution statement

Beatrice Gatto: Formal analysis, Visualization, Data curation, Writing - Original Draft. **Davide Furlanetto**: Formal analysis, Visualization, Writing - Review & Editing. **Matteo Camporese**: Conceptualization, Methodology, Supervision, Writing - Review & Editing. **Tommaso Trentin**: Data curation, Writing - Review & Editing. **Paolo Salandin**: Funding acquisition, Writing - Review & Editing.

Declaration of Competing Interest

The authors declare that they have no known competing financial interests or personal relationships that could have appeared to influence the work reported in this paper.

Data Availability

Data will be made available on request.

Acknowledgments

We gratefully acknowledge the financial support of UniSMART – Fondazione Università degli Studi di Padova and Alto Trevigiano Servizi S.p.A., which funded the doctoral scholarship of the first author. We also thank two anonymous reviewers for their helpful and

constructive comments.

References

Allen, R.G., Pereira, L.S., Raes, D. & Smith, M. (2006). FAO irrigation and drainage Paper No. 56. Crop evapotranspiration (guidelines for computing crop water requirements), 1–333.

ARPAV (2022). Consumo di suolo nella regione Veneto. ⟨https://www.arpa.veneto.it/temi-ambientali/suolo/file-e-allegati/documenti/consumo-di-suolo/consumo-di-suolo-nella-regione-veneto-nel-2021.pdf/@@display-file/file⟩.

Azarnivand, A., Camporese, M., Alaghmand, S., Daly, E., 2020. Modeling hydrological impacts of afforestation on intermittent streams. Sci. Total Environ. 728, 138748 https://doi.org/10.1016/j.scitotenv.2020.138748.

Barbi, A., Cola, G. & Mariani L. (2011). *Inquadramento climatico del Veneto*. Centro Meteorologico di Teolo (PD) ARPAV, Dipartimento Regionale Sicurezza del Territorio. Dipartimento Produzioni Vegetali, Sezione Agronomia, Facoltà di Agraria Università degli Studi di Milano.

Bizhanimanzar, M., Leconte, R., Nuth, M., 2019. Modelling of shallow water table dynamics using conceptual and physically based integrated surface-water–groundwater hydrologic models. Hydrol. Syst. Sci. 23, 2245–2260. https://doi.org/10.5194/hess-23-2245-2019.

Bizhanimanzar, M., Leconte, R., Nuth, M., 2020. Catchment-scale integrated surface water-groundwater hydrologic modelling using conceptual and physically based models: a model comparison study. Water 12, 363. ⟨https://www.mdpi.com/2073-4441/12/2/363⟩.

Boretti, A., Rosa, L., 2019. Reassessing the projections of the world water development report. npj Clean. Water 2, 15. https://doi.org/10.1038/s41545-019-0039-9.

Brunner, P., Simmons, C.T., 2012. HydroGeoSphere: a fully integrated, physically based hydrological model. Groundwater 50 (2), 170–176. https://doi.org/10.1111/j.1745-6584.2011.00882.x.

Camporese, M., Paniconi, C., Putti, M., Orlandini, S., 2010. Surface-subsurface flow modeling with path-based runoff routing, boundary condition-based coupling, and assimilation of multisource observation data. Water Resour. Res. 46 (2), W02512. https://doi.org/10.1029/2008WR007536.

Camporese, M., Daly, E., Dresel, P.E., Webb, J.A., 2014. Simplified modeling of catchment-scale evapotranspiration via boundary condition switching. ISSN 0309-1708 Adv. Water Resour. 69, 95–105. https://doi.org/10.1016/j.advwatres.2014.04.008.

Camporese, M., Daly, E., Paniconi, C., 2015. Catchment-scale Richards equation-based modeling of evapotranspiration via boundary condition switching and root water uptake schemes. Water Resour. Res. 51, 5756–5771. https://doi.org/10.1002/2015WR017139.

Camporese, M., Paniconi, C., Putti, M., McDonnell, J.J., 2019. Fill and spill hillslope runoff representation with a Richards equation-based model. Water Resour. Res. 55, 8445–8462. https://doi.org/10.1029/2019WR025726.

Carsel, R.F., Parrish, R.S., 1988. Developing joint probability distributions of soil water retention characteristics. Water Resour. Res. 24 (5), 755–769. https://doi.org/10.1029/WR024i005p00755.

Dal Prà, A., Martignago, G., Niceforo, U., Tamaro, M., Vielmo, A. & Zannin A. (1996). *Il contributo delle acque irrigue alla ricarica delle falde nella pianura alluvionale tra Brenta e Piave. L'Acqua n° 4.* ⟨https://www.idrotecnicaitaliana.it/wp-content/uploads/2021/01/DalPra-et-al.-LAcqua-n.–4-1996.pdf⟩.

Deflussi Ecologici Decree 30/2017 (Decreto del Ministero dell'Ambiente e della Tutela e del Territorio e del Mare).

Diersch, Hans-J.örg, 2013. FEFLOW—Finite Element Modeling of Flow, Mass and Heat Transport in Porous and Fractured Media. Springer Berlin, Heidelberg. https://doi.org/10.1007/978-3-642-38739-5.

Doherty, J. (2015). *Calibration and Uncertainty Analysis for Complex Environmental Models*. Watermark Numerical Computing, Brisbane, Australia. ISBN: 978–0-9943786–0-6.

Duan, Q., Sorooshian, S., Gupta, V.K., 1994. Optimal use of the SCE-UA global optimization method for calibrating watershed models. J. Hydrol. 158 (3–4), 265–284. https://doi.org/10.1016/0022-1694(94)90057-4.

Edmunds, W.M. & Shand, P. (2008). *Natural Groundwater Quality*. Blackwell Publishing Ltd European Drinking Water Directive 2020/2184.

Fabbri, P., Piccinini, L., Marcolongo, E., Pola, M., Conchetto, E., Zangheri, P., 2016. Does a change of irrigation technique impact on groundwater resources? A case study in Northeastern Italy. issn: 18736416 Environ. Sci. Policy 63, 63–75. https://doi.org/10.1016/j.envsci.2016.05.009.

Famiglietti, J., 2014. The global groundwater crisis. Nat. Clim. Change 4. https://doi.org/10.1038/nclimate2425.

Fatichi, S., Vivoni, E.R., Ogden, F.L., Ivanov, L.Y., Mirus, B., Gochis, D., Downer, C.W., Camporese, M., Davison, J.H., Ebel, B., Jones, N., Kim, J., Mascaro, G., Niswonger, R., Restrepo, P., Rigon, R., Shen, C., Sulis, M., Tarboton, D., 2016. An overview of current applications, challenges, and future trends in distributed process-based models in hydrology. J. Hydrol. 537, 45–60. https://doi.org/10.1016/j.jhydrol.2016.03.026.

Feddes, R.A., Kowalik, P., Kolinska-Malinka, K., Zaradny, H., 1976. Simulation of field water uptake by plants using a soil water dependent root extraction function. J. Hydrol. 31, 13–26. https://doi.org/10.1016/0022-1694(76)90017-2.

Gatel, L., Lauvernet, C., Carluer, N., Weill, S., Tournebize, J., Paniconi, C., 2019. Global evaluation and sensitivity analysis of a physically based flow and reactive transport model on a laboratory experiment. Environ. Model. Softw. 113, 73–83. https://doi.org/10.1016/j.envsoft.2018.12.006.

Gatel, L., Lauvernet, C., Carluer, N., Weill, S., Paniconi, C., 2020. Sobol global sensitivity analysis of a coupled surface/subsurface water flow and reactive solute transfer model on a real hillslope. Water 12 (1), 121. https://doi.org/10.3390/w12010121.

Gatto, B., Paniconi, C., Salandin, P., Camporese, M., 2021. Numerical dispersion of solute transport in an integrated surface–subsurface hydrological model. Adv. Water Resour. 158. https://doi.org/10.1016/j.advwatres.2021.104060.

Gauthier, M.J., Camporese, M., Rivard, C., Paniconi, C., Larocque, M., 2009. A modeling study of heterogeneity and surface water-groundwater interactions in the Thomas Brook catchment, Annapolis Valley (Nova Scotia, Canada). Hydrol. Earth Syst. Sci. 13, 1583–1596. https://doi.org/10.5194/hess-13-1583-2009.

van Genuchten, M.T., 1980. A closed-form equation for predicting the hydraulic conductivity of unsaturated soils. Soil Sci. Soc. Am. J. 44, 892–898.

Gleick, P., Cooley, He, 2021. Freshwater scarcity. Annu. Rev. Environ. Resour. 46. https://doi.org/10.1146/annurev-environ-012220-101319. ⟨https://www.annualreviews.org/doi/pdf/10.1146/annurev-environ-012220-101319⟩.

Gumuła-Kawęcka, A., Jaworska-Szulc, B., Szymkiewicz, A., Gorczewska-Langner, W., Pruszkowska-Caceres, M., Angulo-Jaramillo, R., Šimůnek, J., 2022. Estimation of groundwater recharge in a shallow sandy aquifer using unsaturated zone modeling and water table fluctuation method. ISSN 0022-1694 J. Hydrol. 605, 127283. https://doi.org/10.1016/j.jhydrol.2021.127283.

Haque, A., Salama, A., Lo, K., Wu, P., 2021. Development of an integrated numerical flow model in the Prairie Environment – a case study of the Leech Lake Aquifer system, Saskatchewan, Canada. J. Hydrol.: Reg. Stud. 36, 100869 https://doi.org/10.1016/j.ejrh.2021.100869.

Hossein, T., Kaveh, O.A.A., 2022. Hydro geo-sphere integrated hydrologic model in modeling of wide basins. Sustain. Water Resour. Manag. 8, 118. https://doi.org/10.1007/s40899-022-00689-y.

IRSA-CNR, Gruppo di studio sulle falde acquifere profonde della pianura Padana, 1976. Indagine sulle falde aquifere profonde della pianura Padana. Quad. dell'Ist. di Ric. sulle Acque 28.

Jeon, D.J., Ligaray, M., Kim, M., Kim, G., Lee, G., Pachepsky, Y.A., Cha, D.H., Cho, K.H., 2019. Evaluating the influence of climate change on the fate and transport of fecal coliform bacteria using the modified SWAT model. ISSN 0048-9697 Sci. Total Environ. 658, 753–762. https://doi.org/10.1016/j.scitotenv.2018.12.21.

Konikow, L.F., Kendy, E., 2005. Groundwater depletion: a global problem. Hydrogeol. J. 13, 317–320. https://doi.org/10.1007/s10040-004-0411-8.

Long, S.A., Tachiev, G.I., Fennema, R., Cook, A.M., Sukop, M.C., Wilhelm, M.F., 2015. Modeling the impact of restoration efforts on phosphorus loading and transport through Everglades National Park, FL, USA. Sci. Total Environ. 520, 81–95. https://doi.org/10.1016/j.scitotenv.2015.01.094.

Mahlalela, P.T., Blamey, R.C., Reason, C.J.C., 2019. Mechanisms behind early winter rainfall variability in the southwestern Cape, South Africa. Clim. Dyn. 53, 21–39. https://doi.org/10.1007/s00382-018-4571-y.

Maxwell, R.M., Condon, L.E., Kollet, S.J., 2015. A high-resolution simulation of groundwater and surface water over most of the continental US with the integrated hydrologic model ParFlow v3. Geosci. Model Dev. 8 (3), 923–937. https://doi.org/10.5194/gmd-8-923-2015.

de Melo, M.L.A., de Jong van Lier, Q., 2021. Revisiting the Feddes reduction function for modeling root water uptake and crop transpiration. ISSN 0022-1694 J. Hydrol. 603 (Part B), 126952. https://doi.org/10.1016/j.jhydrol.2021.126952.

Mesfin, M., Arjen, Y.H., 2016. Four billion people facing severe water scarcity. Sci. Adv. 2 (2). ⟨https://www.science.org/doi/10.1126/sciadv.1500323⟩.
Muma, M., Gumiere, S.J., Rousseau, A.N., Scudeler, C., Paniconi, C., 2013. Implementation of a root water extraction module in CATHY: comparison of four empirical root-density distribution models. Procedia Environ. Sci. 19, 57–66. https://doi.org/10.1016/j.proenv.2013.06.007.
Osiemo, M., Ogendi, M., M, G., M'Erimba, C., 2019. Microbial quality of drinking water and prevalence of water-related diseases in Marigat Urban Centre, Kenya. Environ. Health Insights. https://doi.org/10.1177/1178630219836988.
Paniconi, C., Putti, M., 2015. Physically based modeling in catchment hydrology at 50: Survey and outlook. Water Resour. Res. 51 (9), 7090–7129. https://doi.org/10.1002/2015WR017780.
Pertti, A., Chris, S., Hailong, W., Doerthe, T., 2017. Integrated surface-subsurface model to investigate the role of groundwater in headwater catchment runoff generation: a minimalist approach to parameterisation. J. Hydrol. 547, 664–677. https://doi.org/10.1016/j.jhydrol.2017.02.023.
Piccinini, L., Fabbri, P., Pola, M., Marcolongo, E., 2017. An example of aquifer heterogeneity simulation to modeling well-head protection areas. Ital. J. Eng. Geol. Environ. 2017 (Special Issue 2017), 103–115. https://doi.org/10.4408/IJEGE.2017-01.S-10.
Reszler, C., Fank, J., 2016. Unsaturated zone flow and solute transport modelling with MIKE SHE: model test and parameter sensitivity analysis using lysimeter data. Environ. Earth Sci. 75, 253. https://doi.org/10.1007/s12665-015-4881-x. ⟨https://link.springer.com/article/10.1007/s12665-015-4881-x⟩.
Richts, A., Vrba, J., 2016. Groundwater resources and hydroclimatic extremes: mapping global groundwater vulnerability to floods and droughts. Article number: 926 Environ. Earth Sci. 75. https://doi.org/10.1007/s12665-016-5632-3.
Scudeler, C., Pangle, L., Pasetto, D., Niu, G.Y., Volkmann, T., Paniconi, C., Putti, M., Troch, P., 2016. Multiresponse modeling of variably saturated flow and isotope tracer transport for a hillslope experiment at the landscape evolution observatory. Hydrol. Earth Syst. Sci. 20, 4061–4078. https://doi.org/10.5194/hess-20-4061-2016.
Shen, C., Phanikumar, M.S., 2010. A process-based, distributed hydrologic model based on a large-scale method for surface-subsurface coupling. Adv. Water Resour. 33 (12), 1524–1541. https://doi.org/10.1016/j.advwatres.2010.09.002.
Surinaidu, L., 2022. Quantifying stream flows and groundwater response under the climate and land use change through integrated hydrological modelling in a South Indian River basin. Water Secur. 17, 100129 https://doi.org/10.1016/j.wasec.2022.100129.
Trentin, T. (2021). Setup of sensor network and modelling of the aquifer system in the high Venetian plain between Treviso, Padova and Venezia. PhD thesis, University of Padova, Italy.
UNESCO World Assessment Programme, (2023). The United Nations World Water Development Report 2023: partnerships and cooperation for water.
Weill, S., Mazzia, A., Putti, M., Paniconi, C., 2011. Coupling water flow and solute transport into a physically-based surface–subsurface hydrological model. Adv. Water Resour. 34, 128–136. https://doi.org/10.1016/j.advwatres.2010.10.001.
Xiong, H., Wang, Y., Guo, X., Han, J., Ma, C., Zhang, X., 2022. Current status and future challenges of groundwater vulnerability assessment: a bibliometric analysis. J. Hydrol. 615, 128694 https://doi.org/10.1016/j.jhydrol.2022.128694.